

Correlated Production of p and \bar{p} in Au+Au Collisions at $\sqrt{s_{NN}} = 200$ GeV

A. Adare,⁸ S. Afanasiev,²² C. Aidala,⁹ N.N. Ajitanand,⁴⁹ Y. Akiba,^{43,44} H. Al-Bataineh,³⁸ J. Alexander,⁴⁹ A. Al-Jamel,³⁸ K. Aoki,^{28,43} L. Aphecetche,⁵¹ R. Armendariz,³⁸ S.H. Aronson,³ J. Asai,⁴⁴ E.T. Atomssa,²⁹ R. Averbeck,⁵⁰ T.C. Awes,³⁹ B. Azmoun,³ V. Babintsev,¹⁸ G. Baksay,¹⁴ L. Baksay,¹⁴ A. Baldissari,¹¹ K.N. Barish,⁴ P.D. Barnes,³¹ B. Bassalleck,³⁷ S. Bathe,⁴ S. Batsouli,^{9,39} V. Baublis,⁴² F. Bauer,⁴ A. Bazilevsky,³ S. Belikov,^{3,21} R. Bennett,⁵⁰ Y. Berdnikov,⁴⁶ A.A. Bickley,⁸ M.T. Bjorndal,⁹ J.G. Boissevain,³¹ H. Borel,¹¹ K. Boyle,⁵⁰ M.L. Brooks,³¹ D.S. Brown,³⁸ D. Bucher,³⁴ H. Buesching,³ V. Bumazhnov,¹⁸ G. Bunce,^{3,44} J.M. Burward-Hoy,³¹ S. Butsyk,^{31,50} S. Campbell,⁵⁰ J.-S. Chai,²³ B.S. Chang,⁵⁸ J.-L. Charvet,¹¹ S. Chernichenko,¹⁸ J. Chiba,²⁴ C.Y. Chi,⁹ M. Chiu,^{9,19} I.J. Choi,⁵⁸ T. Chujo,⁵⁵ P. Chung,⁴⁹ A. Churnyn,¹⁸ V. Cianciolo,³⁹ C.R. Clevelin,¹⁶ Y. Cobigo,¹¹ B.A. Cole,⁹ M.P. Comets,⁴⁰ P. Constantin,^{21,31} M. Csanád,¹³ T. Csörgő,²⁵ T. Dahms,⁵⁰ K. Das,¹⁵ G. David,³ M.B. Deaton,¹ K. Dehmelt,¹⁴ H. Delagrangé,⁵¹ A. Denisov,¹⁸ D. d'Enterria,⁹ A. Deshpande,^{44,50} E.J. Desmond,³ O. Dietzsch,⁴⁷ A. Dion,⁵⁰ M. Donadelli,⁴⁷ J.L. Drachenberg,¹ O. Drapier,²⁹ A. Drees,⁵⁰ A.K. Dubey,⁵⁷ A. Durum,¹⁸ V. Dzhordzhadze,^{4,52} Y.V. Efremenko,³⁹ J. Egdemir,⁵⁰ F. Ellinghaus,⁸ W.S. Emam,⁴ A. Enokizono,^{17,30} H. En'yo,^{43,44} B. Espagnon,⁴⁰ S. Esumi,⁵⁴ K.O. Eyser,⁴ D.E. Fields,^{37,44} M. Finger,^{5,22} F. Fleuret,²⁹ S.L. Fokin,²⁷ B. Forestier,³² Z. Fraenkel,⁵⁷ J.E. Frantz,^{9,50} A. Franz,³ A.D. Frawley,¹⁵ K. Fujiwara,⁴³ Y. Fukao,^{28,43} S.-Y. Fung,⁴ T. Fusayasu,³⁶ S. Gadrat,³² I. Garishvili,⁵² F. Gastineau,⁵¹ M. Germain,⁵¹ A. Glenn,^{8,52} H. Gong,⁵⁰ M. Gonin,²⁹ J. Gosset,¹¹ Y. Goto,^{43,44} R. Granier de Cassagnac,²⁹ N. Grau,²¹ S.V. Greene,⁵⁵ M. Grosse Perdekamp,^{19,44} T. Gunji,⁷ H.-Å. Gustafsson,³³ T. Hachiya,^{17,43} A. Hadj Henni,⁵¹ C. Haegemann,³⁷ J.S. Haggerty,³ M.N. Hagiwara,¹ H. Hamagaki,⁷ R. Han,⁴¹ H. Harada,¹⁷ E.P. Hartouni,³⁰ K. Haruna,¹⁷ M. Harvey,³ E. Haslum,³³ K. Hasuko,⁴³ R. Hayano,⁷ M. Heffner,³⁰ T.K. Hemmick,⁵⁰ T. Hester,⁴ J.M. Heuser,⁴³ X. He,¹⁶ H. Hiejima,¹⁹ J.C. Hill,²¹ R. Hobbs,³⁷ M. Hohlmann,¹⁴ M. Holmes,⁵⁵ W. Holzmann,⁴⁹ K. Homma,¹⁷ B. Hong,²⁶ T. Horaguchi,^{43,53} D. Hornback,⁵² M.G. Hur,²³ T. Ichihara,^{43,44} K. Imai,^{28,43} M. Inaba,⁵⁴ Y. Inoue,^{45,43} D. Isenhower,¹ L. Isenhower,¹ M. Ishihara,⁴³ T. Isobe,⁷ M. Issah,⁴⁹ A. Isupov,²² B.V. Jacak,⁵⁰ J. Jia,⁹ J. Jin,⁹ O. Jinnouchi,⁴⁴ B.M. Johnson,³ K.S. Joo,³⁵ D. Jouan,⁴⁰ F. Kajihara,^{7,43} S. Kametani,^{7,56} N. Kamihara,^{43,53} J. Kamin,⁵⁰ M. Kaneta,⁴⁴ J.H. Kang,⁵⁸ H. Kanou,^{43,53} T. Kawagishi,⁵⁴ D. Kawall,⁴⁴ A.V. Kazantsev,²⁷ S. Kelly,⁸ A. Khanzadeev,⁴² J. Kikuchi,⁵⁶ D.H. Kim,³⁵ D.J. Kim,⁵⁸ E. Kim,⁴⁸ Y.-S. Kim,²³ E. Kinney,⁸ A. Kiss,¹³ E. Kistenev,³ A. Kiyomichi,⁴³ J. Klay,³⁰ C. Klein-Boesing,³⁴ L. Kochenda,⁴² V. Kochetkov,¹⁸ B. Komkov,⁴² M. Konno,⁵⁴ D. Kotchetkov,⁴ A. Kozlov,⁵⁷ A. Král,¹⁰ A. Kravitz,⁹ P.J. Kroon,³ J. Kubart,^{5,20} G.J. Kunde,³¹ N. Kurihara,⁷ K. Kurita,^{45,43} M.J. Kweon,²⁶ Y. Kwon,^{52,58} G.S. Kyle,³⁸ R. Lacey,⁴⁹ Y.-S. Lai,⁹ J.G. Lajoie,²¹ A. Lebedev,²¹ Y. Le Bornec,⁴⁰ S. Leckey,⁵⁰ D.M. Lee,³¹ M.K. Lee,⁵⁸ T. Lee,⁴⁸ M.J. Leitch,³¹ M.A.L. Leite,⁴⁷ B. Lenzi,⁴⁷ H. Lim,⁴⁸ T. Liška,¹⁰ A. Litvinenko,²² M.X. Liu,³¹ X. Li,⁶ X.H. Li,⁴ B. Love,⁵⁵ D. Lynch,³ C.F. Maguire,⁵⁵ Y.I. Makdisi,³ A. Malakhov,²² M.D. Malik,³⁷ V.I. Manko,²⁷ Y. Mao,^{41,43} L. Mašek,^{5,20} H. Masui,⁵⁴ F. Matathias,^{9,50} M.C. McCain,¹⁹ M. McCumber,⁵⁰ P.L. McGaughey,³¹ Y. Miake,⁵⁴ P. Mikeš,^{5,20} K. Miki,⁵⁴ T.E. Miller,⁵⁵ A. Milov,⁵⁰ S. Mioduszewski,³ G.C. Mishra,¹⁶ M. Mishra,² J.T. Mitchell,³ M. Mitrovski,⁴⁹ A. Morreale,⁴ D.P. Morrison,³ J.M. Moss,³¹ T.V. Moukhanova,²⁷ D. Mukhopadhyay,⁵⁵ J. Murata,^{45,43} S. Nagamiya,²⁴ Y. Nagata,⁵⁴ J.L. Nagle,⁸ M. Naglis,⁵⁷ I. Nakagawa,^{43,44} Y. Nakamiya,¹⁷ T. Nakamura,¹⁷ K. Nakano,^{43,53} J. Newby,³⁰ M. Nguyen,⁵⁰ B.E. Norman,³¹ A.S. Nyanin,²⁷ J. Nystrand,³³ E. O'Brien,³ S.X. Oda,⁷ C.A. Ogilvie,²¹ H. Ohnishi,⁴³ I.D. Ojha,⁵⁵ H. Okada,^{28,43} K. Okada,⁴⁴ M. Oka,⁵⁴ O.O. Omiwade,¹ A. Oskarsson,³³ I. Otterlund,³³ M. Ouchida,¹⁷ K. Ozawa,⁷ R. Pak,³ D. Pal,⁵⁵ A.P.T. Palounek,³¹ V. Pantuev,⁵⁰ V. Papavassiliou,³⁸ J. Park,⁴⁸ W.J. Park,²⁶ S.F. Pate,³⁸ H. Pei,²¹ J.-C. Peng,¹⁹ H. Pereira,¹¹ V. Peresedov,²² D.Yu. Peressounko,²⁷ C. Pinkenburg,³ R.P. Pisani,³ M.L. Porschke,³ A.K. Purwar,^{31,50} H. Qu,¹⁶ J. Rak,^{21,37} A. Rakotozafindrabe,²⁹ I. Ravinovich,⁵⁷ K.F. Read,^{39,52} S. Rembeczki,¹⁴ M. Reuter,⁵⁰ K. Reygers,³⁴ V. Riabov,⁴² Y. Riabov,⁴² G. Roche,³² A. Romana,^{29,*} M. Rosati,²¹ S.S.E. Rosendahl,³³ P. Rosnet,³² P. Rukoyatkin,²² V.L. Rykov,⁴³ S.S. Ryu,⁵⁸ B. Sahlmueller,³⁴ N. Saito,^{28,43,44} T. Sakaguchi,^{3,7,56} S. Sakai,⁵⁴ H. Sakata,¹⁷ V. Samsonov,⁴² H.D. Sato,^{28,43} S. Sato,^{3,24,54} S. Sawada,²⁴ J. Seele,⁸ R. Seidl,¹⁹ V. Semenov,¹⁸ R. Seto,⁴ D. Sharma,⁵⁷ T.K. Shea,³ I. Shein,¹⁸ A. Shevel,^{42,49} T.-A. Shibata,^{43,53} K. Shigaki,¹⁷ M. Shimomura,⁵⁴ T. Shohjoh,⁵⁴ K. Shoji,^{28,43} A. Sickles,⁵⁰ C.L. Silva,⁴⁷ D. Silvermyr,³⁹ C. Silvestre,¹¹ K.S. Sim,²⁶ C.P. Singh,² V. Singh,² S. Skutnik,²¹ M. Slunečka,^{5,22} W.C. Smith,¹ A. Soldatov,¹⁸ R.A. Soltz,³⁰ W.E. Sondheim,³¹ S.P. Sorensen,⁵² I.V. Sourikova,³ F. Staley,¹¹ P.W. Stankus,³⁹ E. Stenlund,³³ M. Stepanov,³⁸ A. Ster,²⁵ S.P. Stoll,³ T. Sugitate,¹⁷ C. Suire,⁴⁰ J.P. Sullivan,³¹ J. Sziklai,²⁵ T. Tabaru,⁴⁴ S. Takagi,⁵⁴ E.M. Takagui,⁴⁷ A. Taketani,^{43,44} K.H. Tanaka,²⁴ Y. Tanaka,³⁶ K. Tanida,^{43,44} M.J. Tannenbaum,³ A. Taranenko,⁴⁹ P. Tarján,¹² T.L. Thomas,³⁷ M. Togawa,^{28,43}

A. Toia,⁵⁰ J. Tojo,⁴³ L. Tomášek,²⁰ H. Torii,⁴³ R.S. Towell,¹ V-N. Tram,²⁹ I. Tserruya,⁵⁷ Y. Tsuchimoto,^{17,43} S.K. Tuli,² H. Tydesjö,³³ N. Tyurin,¹⁸ C. Vale,²¹ H. Valle,⁵⁵ H.W. van Hecke,³¹ J. Velkovska,⁵⁵ R. Vertesi,¹² A.A. Vinogradov,²⁷ M. Virius,¹⁰ V. Vrba,²⁰ E. Vznuzdaev,⁴² M. Wagner,^{28,43} D. Walker,⁵⁰ X.R. Wang,³⁸ Y. Watanabe,^{43,44} J. Wessels,³⁴ S.N. White,³ N. Willis,⁴⁰ D. Winter,⁹ C.L. Woody,³ M. Wysocki,⁸ W. Xie,^{4,44} Y. Yamaguchi,⁵⁶ A. Yanovich,¹⁸ Z. Yasin,⁴ J. Ying,¹⁶ S. Yokkaichi,^{43,44} G.R. Young,³⁹ I. Younus,³⁷ I.E. Yushmanov,²⁷ W.A. Zajc,^{9,†} O. Zaudtke,³⁴ C. Zhang,^{9,39} S. Zhou,⁶ J. Zimányi,^{25,*} and L. Zolin²²

(PHENIX Collaboration)

¹Abilene Christian University, Abilene, TX 79699, U.S.

²Department of Physics, Banaras Hindu University, Varanasi 221005, India

³Brookhaven National Laboratory, Upton, NY 11973-5000, U.S.

⁴University of California - Riverside, Riverside, CA 92521, U.S.

⁵Charles University, Ovocný trh 5, Praha 1, 116 36, Prague, Czech Republic

⁶China Institute of Atomic Energy (CIAE), Beijing, People's Republic of China

⁷Center for Nuclear Study, Graduate School of Science, University of Tokyo, 7-3-1 Hongo, Bunkyo, Tokyo 113-0033, Japan

⁸University of Colorado, Boulder, CO 80309, U.S.

⁹Columbia University, New York, NY 10027 and Nevis Laboratories, Irvington, NY 10533, U.S.

¹⁰Czech Technical University, Zikova 4, 166 36 Prague 6, Czech Republic

¹¹Dapnia, CEA Saclay, F-91191, Gif-sur-Yvette, France

¹²Debrecen University, H-4010 Debrecen, Egyetem tér 1, Hungary

¹³ELTE, Eötvös Loránd University, H - 1117 Budapest, Pázmány P. s. 1/A, Hungary

¹⁴Florida Institute of Technology, Melbourne, FL 32901, U.S.

¹⁵Florida State University, Tallahassee, FL 32306, U.S.

¹⁶Georgia State University, Atlanta, GA 30303, U.S.

¹⁷Hiroshima University, Kagamiyama, Higashi-Hiroshima 739-8526, Japan

¹⁸IHEP Protvino, State Research Center of Russian Federation, Institute for High Energy Physics, Protvino, 142281, Russia

¹⁹University of Illinois at Urbana-Champaign, Urbana, IL 61801, U.S.

²⁰Institute of Physics, Academy of Sciences of the Czech Republic, Na Slovance 2, 182 21 Prague 8, Czech Republic

²¹Iowa State University, Ames, IA 50011, U.S.

²²Joint Institute for Nuclear Research, 141980 Dubna, Moscow Region, Russia

²³KAERI, Cyclotron Application Laboratory, Seoul, South Korea

²⁴KEK, High Energy Accelerator Research Organization, Tsukuba, Ibaraki 305-0801, Japan

²⁵KFKI Research Institute for Particle and Nuclear Physics of the Hungarian Academy of Sciences (MTA KFKI RMKI), H-1525 Budapest 114, POBox 49, Budapest, Hungary

²⁶Korea University, Seoul, 136-701, Korea

²⁷Russian Research Center "Kurchatov Institute", Moscow, Russia

²⁸Kyoto University, Kyoto 606-8502, Japan

²⁹Laboratoire Leprince-Ringuet, Ecole Polytechnique, CNRS-IN2P3, Route de Saclay, F-91128, Palaiseau, France

³⁰Lawrence Livermore National Laboratory, Livermore, CA 94550, U.S.

³¹Los Alamos National Laboratory, Los Alamos, NM 87545, U.S.

³²LPC, Université Blaise Pascal, CNRS-IN2P3, Clermont-Fd, 63177 Aubiere Cedex, France

³³Department of Physics, Lund University, Box 118, SE-221 00 Lund, Sweden

³⁴Institut für Kernphysik, University of Muenster, D-48149 Muenster, Germany

³⁵Myongji University, Yongin, Kyonggido 449-728, Korea

³⁶Nagasaki Institute of Applied Science, Nagasaki-shi, Nagasaki 851-0193, Japan

³⁷University of New Mexico, Albuquerque, NM 87131, U.S.

³⁸New Mexico State University, Las Cruces, NM 88003, U.S.

³⁹Oak Ridge National Laboratory, Oak Ridge, TN 37831, U.S.

⁴⁰IPN-Orsay, Université Paris Sud, CNRS-IN2P3, BP1, F-91406, Orsay, France

⁴¹Peking University, Beijing, People's Republic of China

⁴²PNPI, Petersburg Nuclear Physics Institute, Gatchina, Leningrad region, 188300, Russia

⁴³RIKEN, The Institute of Physical and Chemical Research, Wako, Saitama 351-0198, Japan

⁴⁴RIKEN BNL Research Center, Brookhaven National Laboratory, Upton, NY 11973-5000, U.S.

⁴⁵Physics Department, Rikkyo University, 3-34-1 Nishi-Ikebukuro, Toshima, Tokyo 171-8501, Japan

⁴⁶Saint Petersburg State Polytechnic University, St. Petersburg, Russia

⁴⁷Universidade de São Paulo, Instituto de Física, Caixa Postal 66318, São Paulo CEP05315-970, Brazil

⁴⁸System Electronics Laboratory, Seoul National University, Seoul, South Korea

⁴⁹Chemistry Department, Stony Brook University, Stony Brook, SUNY, NY 11794-3400, U.S.

⁵⁰Department of Physics and Astronomy, Stony Brook University, SUNY, Stony Brook, NY 11794, U.S.

⁵¹SUBATECH (Ecole des Mines de Nantes, CNRS-IN2P3, Université de Nantes) BP 20722 - 44307, Nantes, France

⁵²University of Tennessee, Knoxville, TN 37996, U.S.

⁵³Department of Physics, Tokyo Institute of Technology, Oh-okayama, Meguro, Tokyo 152-8551, Japan

⁵⁴Institute of Physics, University of Tsukuba, Tsukuba, Ibaraki 305, Japan

⁵⁵*Vanderbilt University, Nashville, TN 37235, U.S.*
⁵⁶*Waseda University, Advanced Research Institute for Science and
Engineering, 17 Kikui-cho, Shinjuku-ku, Tokyo 162-0044, Japan*
⁵⁷*Weizmann Institute, Rehovot 76100, Israel*
⁵⁸*Yonsei University, IPAP, Seoul 120-749, Korea*
(Dated: July 7, 2018)

Correlations between p and \bar{p} at transverse momenta typical of enhanced baryon production in Au+Au collisions are reported. The PHENIX experiment measures same and opposite sign baryon pairs in Au+Au collisions at $\sqrt{s_{NN}} = 200$ GeV. Correlated production of p and \bar{p} with the trigger particle from the range $2.5 < p_T < 4.0$ GeV/ c and the associated particle with $1.8 < p_T < 2.5$ GeV/ c is observed to be nearly independent of the centrality of the collisions. Same sign pairs show no correlation at any centrality. The conditional yield of mesons triggered by baryons (and anti-baryons) and mesons in the same p_T range rises with increasing centrality, except for the most central collisions, where baryons show a significantly smaller number of associated mesons. These data are consistent with a picture in which hard scattered partons produce correlated p and \bar{p} in the p_T region of the baryon excess.

PACS numbers: 25.75.Dw

INTRODUCTION

A remarkable feature of relativistic heavy ion collisions at RHIC energies is the enhanced production of baryons and anti-baryons relative to mesons at intermediate transverse momenta ($2 < p_T < 5$ GeV/ c) [1, 2]. In central Au+Au collisions at $\sqrt{s_{NN}} = 200$ GeV the baryon/meson ratio is a factor of three higher than in $p+p$ collisions, while in peripheral Au+Au collisions and in d+Au collisions [3] at the same energy only a small increase ($< 20\%$) is observed. The production of protons and anti-protons at intermediate p_T in Au+Au collisions scales with the number of binary nucleon-nucleon collisions [1], contrary to the suppression of pion production [4]. Similar behavior has been observed for strange baryons (Λ and $\bar{\Lambda}$) and mesons (K_S^0) [5].

In this same momentum range in $p+p$ collisions at the same center of mass energy the dominant production mechanism shifts from soft processes characterized by non-perturbative low momentum transfer scattering to hard scattering processes characterized by large momentum transfer parton-parton scattering followed by fragmentation of the scattered partons into final state hadrons. Pion production in $\sqrt{s_{NN}} = 200$ GeV $p+p$ collisions is reasonably well described by perturbative QCD (pQCD) down to $p_T \approx 2$ GeV [6]. There are large variations in the p and \bar{p} yield among various fragmentation functions which make it difficult to establish a definite pQCD expectation for the p and \bar{p} spectra in $p+p$ collisions [7]. Another estimate of the transition from hard to soft physics can be obtained from the $x_T = 2p_T/\sqrt{s}$ scaling of the single particle cross sections. The cross section can be written as [8, 9]:

$$E \frac{d^3\sigma}{dp^3} = \frac{1}{\sqrt{s}^{n(\sqrt{s}, x_T)}} G(x_T) \quad (1)$$

At high x_T the value of n is found to be independent of both \sqrt{s} and x_T . Since the power of n is related to the

quantum exchanged and the number of point-like scatterers, the x_T region corresponding to the asymptotic n value is understood to be the region where particle production is dominated by hard scattering. Recent measurements of the p and \bar{p} and π^\pm spectra show the cross section can be described by consistent values of n for $p_T > 2$ GeV/ c for both the π^\pm ($n = 6.8 \pm 0.5$) and p and \bar{p} ($n = 6.5 \pm 1.0$) [7] indicating, together with the agreement between the data and pQCD calculations at high p_T [6, 7], that at $\sqrt{s} = 200$ GeV the transition from hard to soft particle production happens at $p_T \approx 2$ GeV/ c . Since the fragmentation process is believed to be independent of center of mass energy or collision system, baryon and anti-baryon production in central Au+Au collisions appears inconsistent with hard-scattering followed by a universal fragmentation.

The theoretical models that are successful in reproducing the measured single particle spectra, baryon/meson ratios and the nuclear modification factors usually invoke some mechanism to extend the range of soft particle production for baryons to higher p_T than that for mesons. This is either done based on the particle mass (in hydrodynamics models [10, 11]) or on the quark content (quark recombination models [12, 13, 14]). An alternative approach, which involves production of baryons through gluon junctions has also been shown to reproduce the data [15]. In this paper we study two-particle angular correlations involving p , \bar{p} , and mesons (π^\pm , K^\pm). This approach gives information about the hadron production in hard-scattering processes, which is inaccessible from single particle measurements.

Previous studies [16, 17, 18] in Au+Au collisions show that at intermediate p_T particles are correlated in azimuthal angle in a manner consistent with jet fragmentation. Namely, particles are emitted close together when they come from fragmentation of the same jet (near side correlations) or approximately back-to-back when they come from the fragmentation of the associated di-

jet (away side correlations). Strong modifications of the yields, shapes and particle composition of these correlations are seen from peripheral to central Au+Au collisions. The yields are quantified by the number of associated particles per trigger (conditional yield) after the combinatorial background from the underlying event has been subtracted. The conditional yield is measured separately for the near and away side correlations. The near side conditional yield increases [16, 17, 18] with centrality and the away side shape has a peak at $\Delta\phi \approx 2$ rad and no peak at $\Delta\phi \approx \pi$ rad. Correlations between identified baryons (p , \bar{p}) and charged hadrons [17] rule out baryon production from $2.5 < p_T < 4.0$ GeV/ c as coming dominantly from a thermal parton source with no correlations. Moreover, the magnitude of baryon and meson triggered correlations with other charged hadrons in the same event is similar, indicating that the baryon excess in the intermediate p_T range is associated with hard parton-parton scattering.

There are two main recombination models which have attempted to address the connection between hard scattering and recombination. The model of Hwa and Yang [14] has calculated that fragmenting partons from hard scattering process have a high probability to recombine with thermal quarks from the medium. The model of Fries *et al.* [19] finds these effects to be unimportant, but has correlations from fast partons losing energy in the medium creating a region around the parton trajectory with a slightly increased temperature and with additional momentum in the direction of the energetic parton. Partons from this region then recombine into hadrons which are correlated with the fast parton direction and with each other.

In order to further explore the jet-like structure of the baryon excess, here we present results on the angular correlations between two identified particles. The baryon production mechanism is studied via correlations between two charge separated p and \bar{p} . If main the source of the baryon excess is jets that fragment outside the medium, the charge dependence of correlations between p and \bar{p} should be the same from peripheral collisions, where baryon production at intermediate p_T is nearly unmodified from p+p collisions, to central collisions. A centrality dependence of the charge combinations of p and \bar{p} correlations would provide evidence for novel baryon production scenarios in central Au+Au collisions.

Correlations between baryon and meson triggers with associated mesons are studied as well. Meson trigger-associated mesons (meson-meson) correlations provide a baseline for jet fragmentation in Au+Au collisions. Separating the baryon-hadron correlations from [17] into baryon-meson and baryon-baryon correlations allows greater sensitivity to possible recombination effects. The recombination model of Fries *et al.* [19] predicts a greater amplification of baryon-baryon correlations relative to baryon-meson correlations on the near side because of

the larger number of possible correlations between the valence quarks.

Near side correlations from jets in p+p collisions are observed to be balanced by away side correlations from the associated di-jet [20]. The away side correlations at intermediate p_T in Au+Au collisions have been shown to have a modified shape in Au+Au collisions [18]. Here we measure the away side correlations with both particles identified in order to see if the dependence on the trigger and associated particle type changes with centrality. If the baryon and meson triggers are from hard scattering with approximately the same momentum transfer, we expect the away side correlations to be independent of the trigger particle type.

The paper is organized as follows: Section describes the experimental method and setup, the results are presented in Section , and Section is devoted to discussion.

EXPERIMENTAL PROCEDURE AND SETUP

Two particle correlations have been widely used to study jets in heavy ion collisions [16, 17, 18, 21, 22] where, due to the high multiplicity and moderate jet energy the direct reconstruction of jets by standard algorithms, utilizing hadronic calorimetry and cluster algorithms, is not yet possible. In this approach particles are divided into two classes, *triggers* and *associated particles*. We classify the triggers and associated particles by their p_T , particle type and charge. The triggers have $2.5 < p_T < 4.0$ GeV/ c and the associated particles have $1.8 < p_T < 2.5$ GeV/ c . Thus both particles originate from a region in p_T that is consistent with hard scattering in $p + p$ collisions and shows an excess of baryons relative to mesons in Au+Au collisions. A distribution of the azimuthal angular difference $\Delta\phi$ between trigger-associated particle pairs is constructed and normalized by the number of triggers.

The data presented here are based on an analysis of 600M Au+Au events collected by the PHENIX experiment in 2004 with a minimum bias trigger. Charged particles are reconstructed in the central arms of PHENIX using a combination of drift chambers and one layer of multi-wire proportional chamber with pad readout (PC1) [23], each covering $\Delta\phi = \pi/2$ in azimuthal angle and $|\eta| < 0.35$ in pseudorapidity. The pattern recognition is based on a combinatorial Hough transform in the track bend plane. The polar angle is determined from the hit position in PC1 and the collision vertex along the beam axis measured by the Beam-Beam Counters (BBC). The BBC are positioned at $|\eta| = 3-4$. Particles are identified by their mass calculated from the measured momentum and time-of-flight information. The global start time is provided by BBC, while the stop time is measured by the PHENIX high resolution time of flight detector (TOF) or the lead-scintillator electromagnetic

calorimeter (EMCal) which provide a 4σ K/p separation up to $p_T \approx 4.0$ GeV/ c and $p_T \approx 2.5$ GeV/ c , respectively. The trigger particles are identified in the TOF, which covers a portion of the PHENIX East arm ($\Delta\phi = \pi/4$). The associated particles are identified in either the EMCAL or the TOF, which together cover the entire PHENIX azimuthal acceptance. For both triggers and associated particles a 2σ spatial match is required between the track projection and the hit position in the particle identification detector. Monte Carlo studies have shown that, due to the decay kinematics in the trigger and partner p_T range used here, the contribution from $\Lambda \rightarrow p\pi^-$ and $\bar{\Lambda} \rightarrow \bar{p}\pi^+$ resonance decays, which could produce correlations mimicking the jet signal, is negligible.

We perform a correction for the non-uniform pair acceptance in $\Delta\phi$ in PHENIX. This correction is constructed by measuring the $\Delta\phi$ distribution from trigger-associated particle pairs where each particle comes from a different event. Dividing the same-event by the mixed-event distribution removes the effects of the PHENIX acceptance and leaves only the true correlations. The multiplicity of the combinatorial background of the underlying event is determined absolutely by the convolution of the measured trigger and associated particle single particle rates with an additional correction for centrality correlations [17] which raises the combinatorial background level by $\approx 0.2\%$ in the most central collisions and $\approx 25\%$ in peripheral collisions. A correction for the associated particle reconstruction efficiency and acceptance is applied by matching the observed rates for the corresponding single particle spectra measured in [2]. No correction has been made for p and \bar{p} originating from weak decays of Λ and $\bar{\Lambda}$; approximately 30% of the measured p and \bar{p} are from these decays [2]. The PHENIX η acceptance is narrow compared to the width of the typical jet cone in p+p collisions [20], so we do not measure the entire conditional yield associated with the trigger particle in the associated particle p_T range. The results are reported for both trigger and associated particles within $|\eta| < 0.35$ without extrapolating in pseudorapidity. The centrality dependence of the conditional yields allows us to quantify changes in the jet-like correlations as a function of centrality and particle type, despite the limited acceptance.

Elliptic flow is an azimuthal correlation between particles due to the anisotropy in the initial collision geometry. This angular correlation is unrelated to jet fragmentation and thus produces a background for this measurement. The correlations due to elliptic flow are removed by modulating the azimuthally uniform combinatorial background by $1 + 2v_2^{trig}v_2^{part} \cos(\Delta\phi)$ where v_2^{trig} and v_2^{part} represent the strength of the elliptic flow signal for the trigger and associated particle, respectively. The v_2 parameter is defined by the 2nd harmonic azimuthal anisotropy, $v_2 = \langle \cos[2(\phi - \Psi)] \rangle$, where ϕ is the azimuthal angle of emitted particle, Ψ is the az-

imuthal angle of event plane in a given collision, and the bracket denotes the average over all particles and events [24]. We measure v_2 of charged baryons and mesons at mid-rapidity, $|\eta| < 0.35$, for each centrality and p_T bin through the event plane method [24]. The azimuthal angle of the event plane is determined by the BBC using the elliptic moment definition [25]. The large rapidity difference, $|\Delta\eta| \sim 3$, between the central arms and the BBCs helps to reduce the non-flow contributions to the measured v_2 , especially those arising from dijets. The systematic errors on the v_2 value are dominated by the uncertainty in the correction for the event plane resolution [25]. The v_2 values used in this analysis are shown in Table I. They are consistent with prior PHENIX v_2 measurements [25] in the common centrality bins. The analysis has been performed separately for associated particles in two transverse momentum ranges: $1.8 < p_T < 2.0$ GeV/ c and $2.0 < p_T < 2.5$ GeV/ c . This minimizes effects due to the variation of v_2 over the width of the associated particle p_T bin. In order to minimize the statistical errors, the results shown here are a sum of the two bins.

The systematic errors on the conditional yields are due to the systematic and statistical uncertainties on the v_2 values, the uncertainty in the corrections for the centrality correlations in the combinatorial background and in the centrality dependence of the efficiency corrections. The systematic error on the centrality dependence of the efficiency corrections is 6% for meson associated particles and 5% for inclusive p , \bar{p} and baryon (p and \bar{p} combined) associated particles independent of centrality. The size of the systematic error on the conditional yield attributed to a systematic uncertainty in the elliptic flow determination is largest in the most central collisions. The systematic error on the centrality correlations is $\approx 60\%$ of the correction in central collisions and $\approx 5\%$ of the correction in peripheral collisions. There are additional systematic errors which are not shown in the figures in Section that come from the centrality independent normalization of the efficiency corrections and move all points with the same associated particle type together. These are 8.9% for p and \bar{p} associated particles, 11.4% for baryon (p and \bar{p}) associated particles, and 13.6% for meson associated particles.

RESULTS

Our goal is to study the jet contribution to baryon and anti-baryon production at intermediate p_T where an excess of baryons over mesons is observed. Thus we choose trigger baryons from the range $2.5 < p_T < 4.0$ GeV/ c and associated particles in the range $1.8 < p_T < 2.5$ GeV/ c and construct two-particle azimuthal correlation distributions. With the larger data sample obtained in 2004 we are able to extend our previ-

TABLE I: The v_2 values and statistical and systematic errors for the centrality and p_T bins used in the analysis.

Centrality	v_2 Values \pm Statistical Error \pm Systematic Error		
	Triggers $2.5 < p_T < 4.0$ GeV/c	Associated Particles $1.8 < p_T < 2.0$ GeV/c	Associated Particles $2.0 < p_T < 2.5$ GeV/c
Baryons			
0-5%	$0.083 \pm 0.006 \pm 0.017$	$0.064 \pm 0.004 \pm 0.013$	$0.068 \pm 0.004 \pm 0.014$
5-10%	$0.126 \pm 0.005 \pm 0.016$	$0.089 \pm 0.003 \pm 0.011$	$0.108 \pm 0.003 \pm 0.013$
10-20%	$0.176 \pm 0.003 \pm 0.013$	$0.134 \pm 0.002 \pm 0.010$	$0.154 \pm 0.002 \pm 0.011$
20-40%	$0.234 \pm 0.003 \pm 0.014$	$0.182 \pm 0.002 \pm 0.011$	$0.203 \pm 0.002 \pm 0.012$
40-60%	$0.264 \pm 0.006 \pm 0.015$	$0.211 \pm 0.004 \pm 0.012$	$0.235 \pm 0.004 \pm 0.013$
60-90%	$0.276 \pm 0.033 \pm 0.044$	$0.158 \pm 0.023 \pm 0.025$	$0.179 \pm 0.021 \pm 0.029$
Mesons			
0-5%	$0.072 \pm 0.007 \pm 0.015$	$0.067 \pm 0.003 \pm 0.014$	$0.078 \pm 0.003 \pm 0.016$
5-10%	$0.109 \pm 0.005 \pm 0.014$	$0.102 \pm 0.002 \pm 0.013$	$0.103 \pm 0.002 \pm 0.013$
10-20%	$0.142 \pm 0.003 \pm 0.011$	$0.133 \pm 0.001 \pm 0.010$	$0.140 \pm 0.001 \pm 0.010$
20-40%	$0.185 \pm 0.003 \pm 0.011$	$0.172 \pm 0.001 \pm 0.010$	$0.180 \pm 0.001 \pm 0.011$
40-60%	$0.186 \pm 0.006 \pm 0.010$	$0.188 \pm 0.003 \pm 0.011$	$0.191 \pm 0.003 \pm 0.011$
60-90%	$0.178 \pm 0.027 \pm 0.029$	$0.173 \pm 0.013 \pm 0.028$	$0.172 \pm 0.014 \pm 0.028$

ous studies [17] by studying the proton and anti-proton triggers, as well as identifying the associated particles. Several combinations of trigger-associated particle types are presented below.

We first study baryon-baryon correlation, where both trigger and associated particles are identified as either p or \bar{p} . The left panel of Figure 1 shows the azimuthal angular difference, $\Delta\phi$, between charge inclusive p and \bar{p} measured in six centrality classes. The solid lines show the combinatorial background level modulated by the expected correlation due to elliptic flow, $B(1 + 2v_2^{trig}v_2^{assoc} \cos(2\Delta\phi))$. The excess is attributed to jet correlations, $J(\Delta\phi)$. The azimuthal angular difference distributions are then described by:

$$\frac{1}{N_{trig}} \frac{dN}{d\Delta\phi} = B(1 + 2v_2^{trig}v_2^{assoc} \cos(2\Delta\phi)) + J(\Delta\phi). \quad (2)$$

The region around $\Delta\phi = \pi/2$ has very limited acceptance for pairs due to the requirement that the trigger particle be measured in the TOF detector. The right panels of Figure 1 show the $J(\Delta\phi)$ for three centralities after the combinatorial background subtraction. There is a pronounced jet peak at small relative angles (near side), however, there is no visible structure on the away side, where the yields are slightly above or at the level of the combinatorial background.

To further explore the observed structures, in Figures 2 and 3 we perform the analysis separately for each charge combination. The correlations were measured in the same p_T range as in Figures 1. A near side excess can be seen over the combinatorial background for opposite sign pairs (left panel of Figure 2 and right panel of Fig-

ure 3) while no significant excess is seen for the same sign pairs (right panel of Figure 2 and left panel of Figure 3).

The correlations involving mesons as associated particles provide a comparison baseline for the baryon-baryon correlations. We study both baryon and meson triggers associated with mesons. The left panel of Figure 4 shows the baryon-meson and meson-meson correlations. The right panels of Figure 4 show $J(\Delta\phi)$ for the 0-5%, 20-40% and 60-90% centrality classes. While in the mid-central collisions the meson and baryon triggered distributions agree well, the baryon triggered distributions in the most central collisions lie systematically below the meson triggered points both before and after the combinatorial background subtraction on the near side.

To quantify the observed differences in the various trigger-associated particle combinations, we integrate the $J(\Delta\phi)$ distributions in the regions $0.0 < \Delta\phi < 0.94$ rad and $\pi - 0.94 < \Delta\phi < \pi$ rad to obtain the near-side and the away-side conditional yields, respectively. Figures 5 and 6 show the conditional yield per trigger as a function of the number participating nucleons (N_{part}). The results were obtained from the data in Figures 2 and 3 (solid points) and Figure 1 (open points) by integrating the $J(\Delta\phi)$ in the $\Delta\phi$ ranges specified above. This integration range excludes a large part of the away side shape modifications observed in [18]. The small integration range is used in this analysis only because of the limited acceptance around $\Delta\phi = \pi/2$ due to the requirement to measure the trigger particle in the TOF. These results quantify the centrality and particle type dependence of the jet-like correlations. Figure 5 shows that the correlations between opposite sign baryon pairs

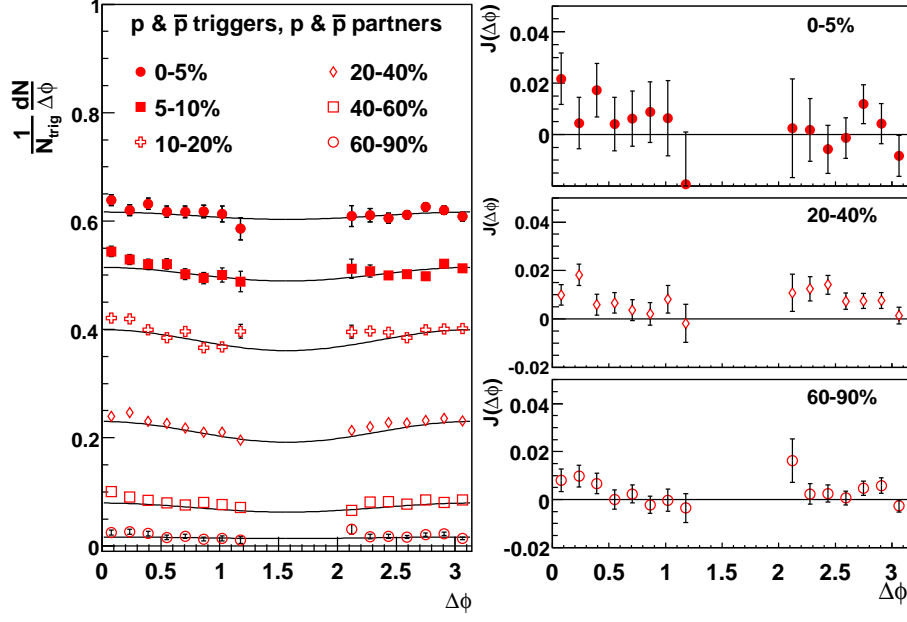


FIG. 1: Left: $\frac{1}{N_{trig}} \frac{dN}{d\Delta\phi}$ distributions for charge-inclusive baryon triggers and associated particles for six centrality bins. Triggers have $2.5 < p_T < 4.0$ GeV/c and associated particles have $1.8 < p_T < 2.5$ GeV/c. The solid lines indicate the combinatorial background modulated by elliptic flow. Right: Jet distributions, $J(\Delta\phi)$, after combinatorial background and elliptic flow subtraction for 0-5% (top), 20-40% (middle) and 60-90% (bottom) centralities. In all panels, only the statistical errors are shown.

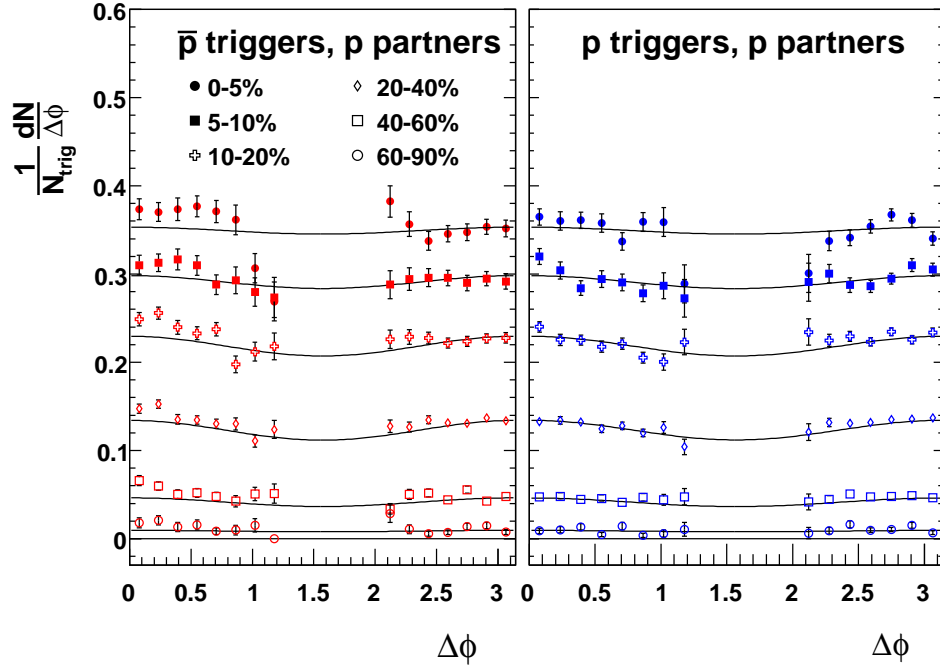


FIG. 2: $\frac{1}{N_{trig}} \frac{dN}{d\Delta\phi}$ distributions for charge selected \bar{p} (left) and p (right) triggers both with associated p for six centrality bins. Triggers have $2.5 < p_T < 4.0$ GeV/c and associated particles have $1.8 < p_T < 2.5$ GeV/c. The solid lines indicate the combinatorial background modulated by elliptic flow. Only the statistical errors are shown.

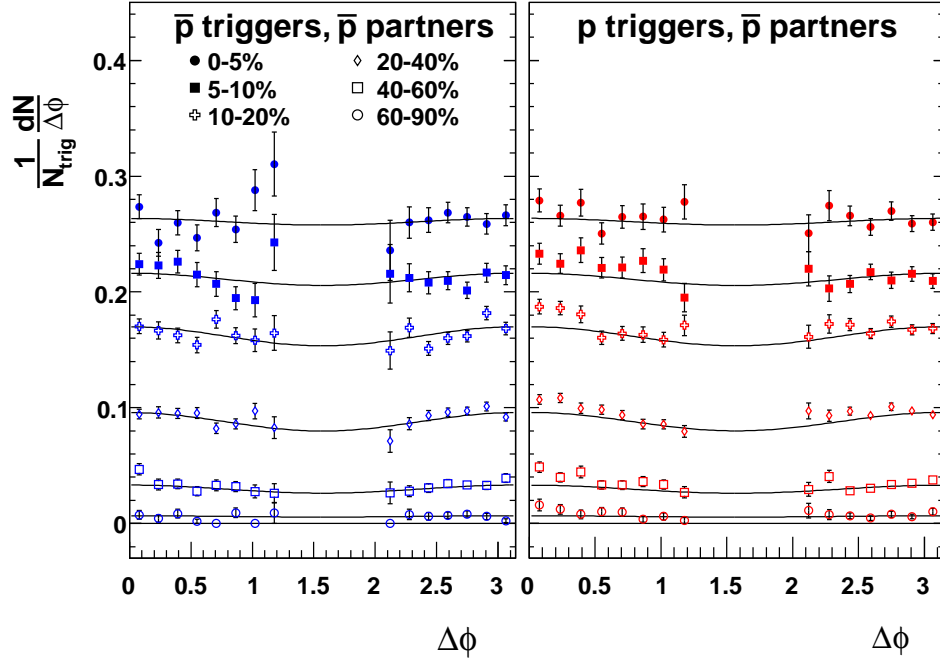


FIG. 3: $\frac{1}{N_{trig}} \frac{dN}{d\Delta\phi}$ distributions for charge selected \bar{p} (left) and p (right) triggers both with associated \bar{p} for six centrality bins. Triggers have $2.5 < p_T < 4.0$ GeV/c and associated particles have $1.8 < p_T < 2.5$ GeV/c. The solid lines indicate the combinatorial background modulated by elliptic flow. Only the statistical errors are shown.

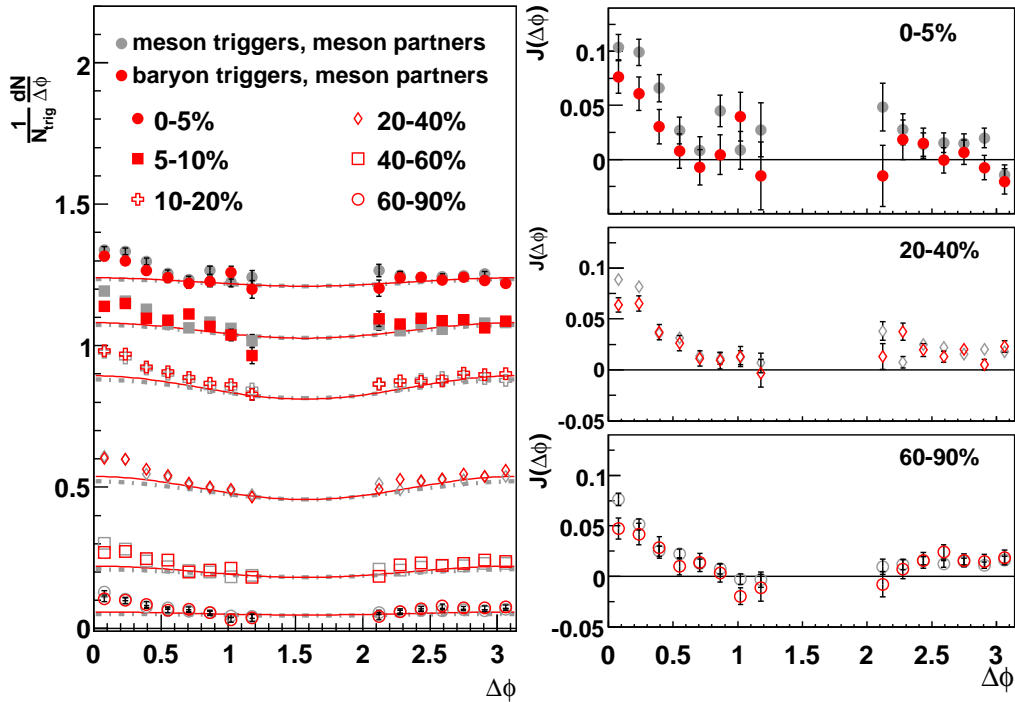


FIG. 4: Left: $\frac{1}{N_{trig}} \frac{dN}{d\Delta\phi}$ distributions for charge-inclusive baryon and meson triggers and associated mesons for six centrality bins. Triggers have $2.5 < p_T < 4.0$ GeV/c and associated particles have $1.8 < p_T < 2.5$ GeV/c. The solid lines indicate the combinatorial background modulated by elliptic flow. Right: Jet distributions, $J(\Delta\phi)$, after combinatorial background and elliptic flow subtraction for 0-5% (top), 20-40% (middle) and 60-90% (bottom) centralities. In all panels, only the statistical errors are shown.

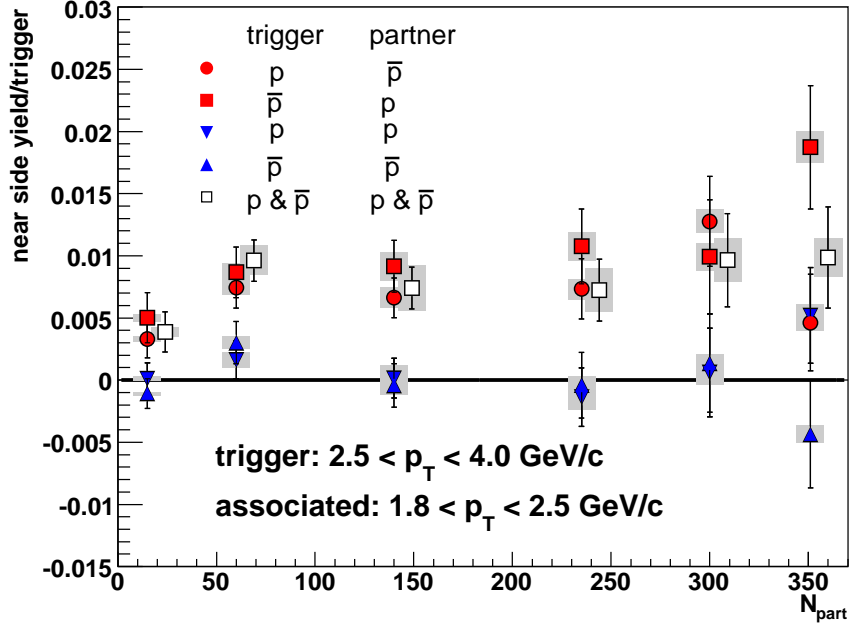


FIG. 5: Conditional yields per trigger on the near side for charge selected (solid points) and charge selected (hollow points) p and \bar{p} correlations. Triggers have $2.5 < p_T < 4.0 \text{ GeV}/c$ and associated particles have $1.8 < p_T < 2.5 \text{ GeV}/c$. The error bars are the statistical errors and the boxes show the systematic errors. There is an 11.4% additional normalization error on baryon associated particle points and 8.9% each on the p and \bar{p} associated particle points.

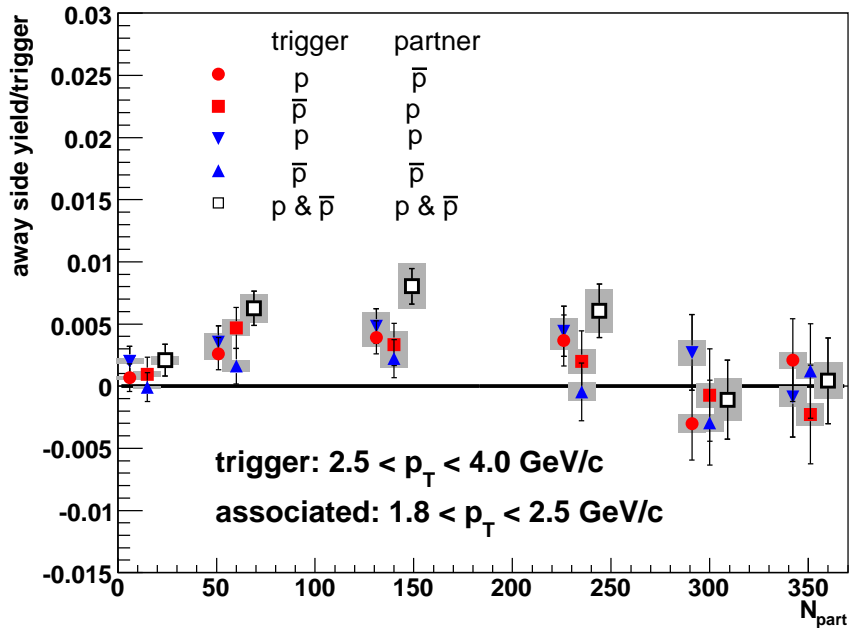


FIG. 6: Conditional yields per trigger on the away side for charge selected (solid points) and charge selected (hollow points) p and \bar{p} correlations. Triggers have $2.5 < p_T < 4.0 \text{ GeV}/c$ and associated particles have $1.8 < p_T < 2.5 \text{ GeV}/c$. The error bars are the statistical errors and the boxes show the systematic errors. The additional normalization error is the same as in Figure 5.

produce a significant non-zero conditional yield that is nearly independent of centrality and that there is no significant yield associated with same sign pairs. The open points in Figure 5 are from the charge inclusive analysis and show that the conditional yield does come mainly from opposite sign pairs. For all but the most peripheral point, no centrality dependence is observed in the charge inclusive analysis. The most peripheral point sits 2.5σ below the average conditional yield for the other centrality bins. The charge inclusive data are also consistent with a linear increase with N_{part} . The systematic errors on these distributions are highly correlated since the v_2 values and centrality correlation corrections are the same for all points at a given centrality. There is an 8.6% systematic error on the relative normalizations of the associated particle p and \bar{p} points which is not shown. Figure 6 shows the same correlations as Figure 5 for the away side region. Here the charge inclusive points lie above the charge selected points for peripheral and mid-central collisions because both same and opposite charge pairs have non-zero conditional yield. The conditional yield rises from peripheral to mid-central collisions. In the most central collisions both the charge inclusive and charge selected points are consistent with zero.

Figure 7 shows both the near and away side conditional yield for baryon triggers and associated mesons and meson triggers with associated mesons. The meson trigger-associated mesons conditional yield on the near side rises smoothly with centrality. The baryon triggered yields are systematically lower than the meson triggered yields, but also rise linearly with N_{part} for $N_{part} < 250$. In central collisions the baryon triggered yields are lower than the linear N_{part} dependence observed in the meson-meson points for all N_{part} and the baryon-meson points for $N_{part} < 250$. The statistical errors on baryon-meson conditional yields exclude a linear increase with N_{part} on the 2.6σ level. The systematic errors on the v_2 values and the centrality correlation correction are correlated with centrality. The most central baryon triggered point is consistent with the most peripheral baryon triggered point. The most central meson-meson conditional yield is $70\% \pm 20\%$ greater than in peripheral collisions. On the away side, no significant dependence on trigger type is observed.

DISCUSSION

The observed x_T scaling and pQCD calculations suggest hard scattering is the dominant mechanism for particle production for $p_T > 2$ GeV/c at $\sqrt{s}=200$ GeV in p+p collisions [7]. π^0 production in Au+Au collisions at $\sqrt{s_{NN}} = 200$ GeV follows x_T scaling [26] and is well described by perturbative theories which include radiative energy loss by hard partons traversing the medium [27, 28, 29] at p_T as low as 2 GeV/c. Models

which describe the excess of baryons relative to mesons [1] typically do so by some mechanism which extends the p_T range of soft physics. Here we have used two particle azimuthal correlations to study the particle type dependence of jet-like correlations in Au+Au collisions in the region of the baryon excess. Since jets in $e^+ + e^-$ collisions fragment dominantly into mesons [30], we take meson-meson correlations as a baseline for jet fragmentation in Au+Au collisions. The increase in meson-meson near side conditional yield with centrality seen in Figure 7 has also been observed in meson-hadron correlations [17] and hadron-hadron correlations [16, 18] and is not yet quantitatively understood. Here we are interested primarily in jet correlations of baryons so meson-meson correlations provide a useful reference. The yield of associated mesons per trigger baryon is systematically lower than the yield of associated mesons per trigger meson, but baryon-meson correlations on the near side increase as meson-meson correlations for all centralities except for the most central. On the away side there is no significant dependence on the trigger type for associated mesons, as is expected if baryon and meson triggers come from jets of approximately the same energy and if the di-jets fragment independently of the trigger jet. The yield of associated baryons per baryon trigger on the near side is observed to be nearly constant with centrality, except for the most peripheral point which is significantly lower than the others. The data are also consistent with a linear increase in the conditional yield as a function of N_{part} . The small yield of associated baryons per baryon trigger does not imply that baryon number is not conserved within the near side jet since the p_T range of the measured associated particles is narrow, and the PHENIX η acceptance does not contain all of the associated particles.

The data presented here are consistent with baryons at $2.5 < p_T < 4.0$ GeV/c arising predominately from hard scattering processes. First, the yield of mesons associated with baryon triggers has the same centrality dependence as associated mesons per meson trigger for $N_{part} < 250$ despite a change in the \bar{p}/π^- ratio by a factor of three from peripheral collisions. Second, the away side yield into 0.94 rad is independent of the trigger type, consistent with the away side jet fragmenting independently of the trigger jet. Lastly, the charge dependence of p and \bar{p} correlations show that small angle p - \bar{p} pairs are correlated beyond the expected correlations from elliptic flow, and that small angle p - p and \bar{p} - \bar{p} pairs are not. This is true in peripheral collisions where the \bar{p}/π^- ratio is close to the value from p+p collisions [3] and also in central collisions where the ratio is a factor of three larger. This indicates that the mechanism producing the baryon excess is also producing small angle p - \bar{p} pairs.

The results for near side conditional yields presented here disagree with the recombination model calculation in [31] which predicts a very weak centrality dependence

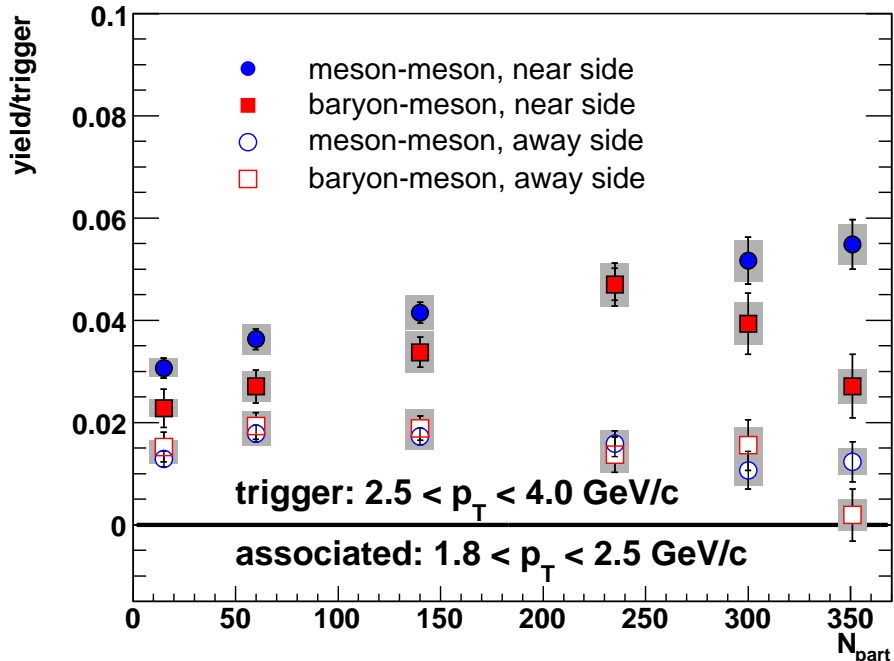


FIG. 7: Conditional yields per trigger for baryon (squares) and meson (circles) triggers with associated mesons. Triggers have $2.5 < p_T < 4.0$ GeV/ c and associated particles have $1.8 < p_T < 2.5$ GeV/ c . The error bars are the statistical errors and the boxes show the systematic errors. There is an additional 13.6% normalization error.

for meson-meson and baryon-meson conditional yields and nearly the same magnitude for baryon-meson and baryon-baryon near side conditional yields. In contrast, the data show the conditional yield of associated mesons with baryon triggers to be a factor of two to five times larger than the conditional yield of baryons associated with baryon triggers, depending on centrality. The results presented here also appear to exclude baryon production via higher twist mechanisms [32] which would produce isolated p and \bar{p} . No correlation calculations are available from the gluon junction model [15], so a comparison beyond the successfully described single particle data could not be done at this point.

We have systematically explored the particle type dependence of jet fragmentation at intermediate p_T in Au+Au collisions at $\sqrt{s_{NN}} = 200$ GeV. The new data disagree with calculations from the recombination model presented in [19, 31]. Given the success of recombination models in reproducing elliptic flow and hadron spectra data it would be interesting to see if other recombination calculations are able to describe the data presented here. We find that near side correlations between meson triggers and associated mesons increase with centrality. Near side correlations between baryon triggers and associated mesons show the same centrality dependence except for the most central collisions where there is a significant decrease. The first measurements of baryon pairs on the

near side are found to be largely due to opposite charge p - \bar{p} pairs. Under the assumption that the above centrality dependencies of particle pairs and single particles are not coincidental, one can explain the observed baryon excess at intermediate p_T in Au+Au collisions via jet induced production of baryon-antibaryon pairs.

We thank the staff of the Collider-Accelerator and Physics Departments at BNL for their vital contributions. We acknowledge support from the Department of Energy and NSF (U.S.A.), MEXT and JSPS (Japan), CNPq and FAPESP (Brazil), NSFC (China), MSMT (Czech Republic), IN2P3/CNRS, and CEA (France), BMBF, DAAD, and AvH (Germany), OTKA (Hungary), DAE (India), ISF (Israel), KRF and KOSEF (Korea), MES, RAS, and FAAE (Russia), VR and KAW (Sweden), U.S. CRDF for the FSU, US-Hungarian NSF-OTKA-MTA, and US-Israel BSF.

* Deceased

† PHENIX Spokesperson: zajc@nevis.columbia.edu

- [1] S. S. Adler, et al., Phys. Rev. Lett 91 (2003) 172301.
- [2] S. S. Adler, et al., Phys. Rev. C69 (2004) 034909.
- [3] S. S. Adler, et al., Phys. Rev. C74 (2006) 024904.
- [4] S. S. Adler, et al., Phys. Rev. Lett 91 (2003) 072301.
- [5] J. Adams, et al., Phys. Rev. Lett. 92 (2004) 052302.

- [6] S. S. Adler, et al., Phys. Rev. Lett. 91 (2003) 241803.
- [7] J. Adams, et al., Phys. Lett. B637 (2006) 161–169.
- [8] S. Berman, J. Bjorken, J. Kogut, Phys. Rev. D4 (1971) 3388.
- [9] R. Blankenbecler, S. Brodsky, J. Gunion, Phys. Lett B42 (1972) 461.
- [10] D. Teaney, J. Lauret, E. V. Shuryak, nucl-th/0110037.
- [11] T. Hirano, Y. Nara, Phys. Rev. C69 (2004) 034908.
- [12] V. Greco, et al., Phys. Rev. C68 (2003) 034904.
- [13] R. J. Fries, et al., Phys. Rev. C68 (2003) 044902.
- [14] R. Hwa, C. B. Yang, Phys. Rev. C70 (2004) 024904.
- [15] V. Topor Pop, M. Gyulassy, J. Barrette, C. Gale, Phys. Rev. C72 (2005) 054901.
- [16] C. Adler, et al., Phys. Rev. Lett. 90 (2003) 082302.
- [17] S. S. Adler, et al., Phys. Rev C71 (2005) 051902(R).
- [18] S. S. Adler, et al., Phys. Rev. Lett. 97 (2006) 052301.
- [19] R. J. Fries, et al., Phys. Rev. Lett 94 (2005) 122301.
- [20] S. S. Adler, et al., Phys. Rev. D74 (2006) 072002.
- [21] C. Adler, et al., Phys. Rev. Lett. 95 (2005) 152301.
- [22] C. Adler, et al., nucl-ex/0604018, submitted to Phys. Rev. Lett.
- [23] K. Adcox, et al., NIM A499 (2003) 489–507.
- [24] A. Poskanzer, S. Voloshin, Phys. Rev. C58 (1998) 1671.
- [25] S. S. Adler, et al., Phys. Rev. Lett. 91 (2003) 182301.
- [26] S. S. Adler, et al., Phys. Rev. C69 (2004) 034910.
- [27] I. Vitev, M. Gyulassy, Phys. Rev. Lett 89 (2002) 232301.
- [28] E. Wang, X. Wang, Phys. Rev. Lett 89 (2002) 162301.
- [29] H. Eskola, H. Honkanen, C. Salgado, U. Wiedermann, Nucl Phys. A747 (2005) 511.
- [30] P. Abreu, et al., Eur. Phys. J. C17 (2000) 207–222.
- [31] R. J. Fries, Journal of Physics Conference Series 27 (2005) 70–79.
- [32] S. Brodsky, H. Pirner, J. Raufeisen, Phys. Lett. B637 (2006) 58–63.